

1 **Towards a satellite-based approach to measure eruptive volumes at Mt. Etna using** 2 **Pleiades datasets**

3
4 Proietti C.¹, Coltelli M.¹, Marsella M.², Martino M.², Scifoni S.³, Giannone F.⁴

5 ¹ Istituto Nazionale di Geofisica e Vulcanologia, Osservatorio Etneo, Piazza Roma 2, 95125 Catania, Italy

6 ² Università di Roma La Sapienza, Via Eudossiana 18, 00184 Roma, Italy

7 ³ Serco Italia S.p.A., Via Sciadonna 24-26 00044 Frascati (Roma), Italy

8 ⁴ Università Niccolò Cusano, Via Don Carlo Gnocchi 3, 00166 Roma, Ital

9
10 Corresponding author: Cristina Proietti, cristina.proietti@ingv.it, +39 095 7165822, ORCID: 0000-0003-
11 4827-402X

12 This is a post-peer-review, pre-copyedit version of an article published in Bulletin of Volcanology. The
13 final authenticated version is available online at <https://doi.org/10.1007/s00445-020-01374-8>

14 15 **Abstract**

16 Only a few high precision studies of lava and tephra during simultaneous explosive and effusive activity
17 have so far been undertaken. We carried out such measurements by analysis of a unique and
18 homogeneous multi-temporal dataset of high-resolution satellite optical images. Digital Elevation Models
19 (DEMs) and orthophotos (with 1- and 0.5-m-pixel resolutions respectively) were extracted from six
20 specifically tasked Pleiades tri-stereo pairs of Mt. Etna volcano, between 2011 and 2016. During this
21 period, frequent effusive and explosive events formed lava flow fields and built up the new south-east
22 crater pyroclastic cone. The volumes of lava fields and proximal pyroclastic deposits were measured by
23 comparing the Pleiades DEMs with an aerial photogrammetric DEM updated in 2007. The volumes of all
24 distal deposits were estimated using lava and tephra partitioning from the literature for an Etnean lava
25 fountain. The dense rock equivalent volume of lava and tephra, calculated to be $248.4 \pm 2.1 \times 10^6 \text{ m}^3$ in
26 total, corresponds to an average output rate of $0.98 \text{ m}^3/\text{s}$ over the analysed eight-year period (May 2008–
27 May 2016) and to a multi-event eruption rate of $5.53 \text{ m}^3/\text{s}$ for 520 days of activity. The multi-temporal
28 analysis of high-resolution satellite DEMs, here successfully applied to the well-monitored Etna volcano,
29 demonstrated that the tasking of high resolution satellite images is crucial for fast and effective
30 monitoring during intense volcanic activity (frequent and overlapping eruptive events). This methodology
31 could be used for the monitoring of remote or hazardous volcanoes that are difficult to study by means of
32 repeated field surveys.

33 34 **Keywords**

35 Pleiades satellite, high resolution DEM, Etna volcano, Eruption volume, Magma output rate

36 **Introduction**

37 Rapid and frequent morphological changes on active volcanoes can make it necessary to update
38 topographic data, such as DEMS and orthophotos, over large areas both during and after eruptions to
39 support risk assessment and mitigation actions. Airborne or satellite remote sensing techniques offering
40 three-dimensional (3-D) mapping capability, are preferable to ground-based topographic instruments in
41 order to acquire data covering wider areas from a safe distance, and as frequently and accurately as
42 possible. Satellite observations have an increasingly important role in advancing the understanding of the
43 volcanic behaviour and are especially useful on remote volcanoes where field or airborne surveys are
44 challenging (e.g. Mougini-Mark et al. 1989; Francis and Rotary 2000; Rowland et al. 2003; Bagnardi et
45 al. 2016; Martino et al. 2016; Bonny et al. 2018).

46 Ground-based measurements enable the volume of morphological change, in particular of lava flows,
47 to be quantified through a planimetric approach in which the planimetric area of change is multiplied by
48 an average thickness (Stevens et al. 1999). Global Positioning System (GPS) surveys or close-range
49 orthorectified digital images can be used to measure the area, while thickness can be measured using total
50 stations or GPS and laser rangefinder (e.g. Calvari et al. 1994; Honda and Nagai 2002; Behncke et al.
51 2014; Marsella et al. 2014; Naranjo et al. 2016; Coltelli et al. 2017; Bonny et al. 2018). Lava thicknesses
52 are mostly measured on flow margins and fronts and might not be representative of central thickness due
53 to surface roughness. This discrepancy is even more relevant for long-duration complex lava fields
54 emplaced on irregular topographies. In these cases, the lava morphology is poorly represented by the
55 limited number of measurements and by a simplified segmentation of the flow fields based on the slope of
56 the pre-existing topography, thus the planimetric volume estimation can have an error greater than 20%
57 (Calvari et al. 1994).

58 Aerial and satellite remote sensing techniques enable the area, volume and thickness of morphological
59 change to be quantified through a topographic approach based on the comparison of DEMs acquired
60 before, during and after an eruption (Stevens et al. 1999). Digital photogrammetry is one of the most
61 flexible tools for producing high spatial resolution (Ground Sampling Distance, GSD, from millimetres to
62 meters depending on the viewing distance) DEMs and orthophotos of rough terrain, such as volcanoes,
63 and can provide sub-meter accuracy (Marsella et al. 2009; Dvigalo et al. 2016). However, aerial
64 photogrammetry can be limited by the hazard posed by an active volcano and by the costs and duration
65 (from hours to days) of image acquisition that increase with the total area to be covered and with the
66 requested spatial resolution (a smaller GSD implies a lower flight height, resulting in smaller area on each
67 image and longer acquisition times). These limits are overcome by space-borne Earth Observation (EO)
68 optical sensors acquiring stereo and tri-stereo scenes with meter (Ikonos and Quickbird) to sub-meter
69 (WorldView and Pleiades) GSD, enabling DEMs and orthophotos to be derived at relatively high
70 temporal frequency (hours to days, if using multiple platforms) and meter-level accuracy. In comparison

71 to aerial data, satellite data provide wider coverage from a single pass thanks to a larger swath width, for
72 example 16.4 km and 20 km at nadir for WorldView and Pleiades, respectively. Other satellite sensors
73 acquire datasets with moderate-to-high spatial resolution (~10 to 100 m GSD such as ASTER, SRTM and
74 SPOT) and generally low temporal frequency (revisiting time of 16, 26 and 1–5 days for ASTER, SPOT
75 4, 5 and SPOT 7, respectively).

76 To explore the possibilities of volcano monitoring through specifically tasked acquisitions, from
77 meter-resolution satellite systems, we carried out photogrammetric processing of optical images, most of
78 which were acquired by the Pleiades spacecraft. The twin spacecraft Pleiades-1A and Pleiades-1B, in
79 operation since December 2011 and December 2012, are capable of daily revisits to any point on the
80 globe and of acquiring panchromatic and multi-spectral images with GSD of 0.5 m and 2 m, respectively
81 (Boissin et al. 2012). Image acquisition can be tasked for specific areas and this is especially valuable for
82 volcano monitoring during eruption crises. From a single pass, Pleiades satellites can capture stereoscopic
83 near-nadir looks in addition to classic forward and backward looks (tri-stereo) allowing a better retrieval
84 of height data over terrains with high roughness, steep slopes, and shadows. Pleiades high-resolution
85 DEMs were used for quantifying the 2014–2015 lava field of Fogo Volcano, Cape Verde showing better
86 performance on lava flow surfaces than on ash and cinder (Bagnardi et al. 2016). A 2015 Pleiades DEM
87 was compared with a photogrammetric DEM of 2005 for quantifying the volume of all 2005–2015
88 eruptive products and of the new South-East crater cone (Ganci et al. 2018).

89 In this study, we exploited high-resolution optical images of the Pleiades satellites, acquired after a
90 specific data tasking in the framework of a scientific collaboration within the Space Volcano Observatory
91 with Pleiades (SVOP) project (http://volcano.iterre.fr/svo_projects). This project was aimed at acquiring
92 data for monitoring the morphological changes in hazardous and/or unreachable areas, such as active
93 volcanoes, and for producing results useful to hazard assessment. Mount Etna was selected as the study
94 area because frequent effusive and explosive eruptive events have recently modified its summit
95 morphology, emplacing compound lava fields and building up the New South-East Crater (NSEC)
96 pyroclastic cone. The analysis of a time-series of DEMs and orthophotos, extracted from Pleiades images,
97 allowed us measuring the volumes of effusive and explosive (proximal) products erupted at Etna between
98 2008 and 2016, while quantifying the associated precisions. The distal products were estimated by
99 applying the relationship between the dense rock equivalent volumes of effusive and explosive products
100 that were precisely measured, for the first time, for the 25–26 October 2013 lava fountain on Etna
101 (Andronico et al. 2018). In this way we measured, through a unique methodology, the total volume
102 (effusive and explosive) of magma erupted at Etna, over an 8-year period, and the output rate, which are
103 key data for understanding eruptive behaviours and assessing relative hazards. Quantifying the volume of
104 the different products of a frequently active volcano can be very difficult; previously published work

105 analysing Etna's recent eruptive activity generally evaluated the total volumes by combining
106 measurements obtained with different techniques.

107 The acquisition of optical images of Etna from Pleiades satellites enabled monitoring of the intense
108 volcanic activity, which was characterized by frequent events and overlapping eruptive products. The tri-
109 stereo acquisition, the large swath width and the high resolution of Pleiades images enabled us to directly
110 extract, from a single pass, DEMs and orthophotos (with meter and sub-meter GSD, respectively) of the
111 whole area covered by the eruptive activity and to adequately map different eruptive products. During
112 intense volcanic activity, image tasking is crucial in order to effectively survey the volcano and quantify
113 the related hazard because it enables distinguishing eruptive events separated by few days. The capacity
114 to directly georeference satellite material reduces or eliminates the need to perform field surveys to
115 measure Ground Control Points (GCPs), although they can help improve the georeferencing. Therefore,
116 the acquisition and analysis of tasked satellite optical images is a methodology highly suited to monitor
117 volcanic eruptions, and it is also faster and safer than surveys based on field or aerial data.

118 119 **The 2007–2016 eruptive activity of Mt. Etna**

120 Since 2007, Etna eruptive activity has mainly occurred in its summit area (Fig. 1), particularly in the
121 New South-East Crater (NSEC), while the other craters Bocca Nuova, North East Crater, South-East
122 Crater and Voragine (BN, NEC, SEC and VOR) have been only occasionally active (Fig. 2). Powerful
123 lava fountains occurred at SEC on 4–5 September 2007, 23–24 November 2007 and 10 May 2008,
124 forming ash plumes and lava flows that extended over the upper Valle del Bove (VdB). Between 13 May
125 2008 and 6 July 2009, a lateral effusive eruption from vents close to the summit area produced a
126 compound lava field on VdB that covered the 2007–2008 flows (Behncke et al. 2016). Subsequently,
127 after a period of only minor activity, an intense and frequent succession of discrete explosive and effusive
128 events (Fig. 2) substantially modified Etna's summit morphology between 2011 and 2016. Compound
129 lava flow fields formed on the East, South and West flanks and the NSEC pyroclastic cone rapidly grew
130 on the east flank of SEC (Behncke et al. 2014; De Beni et al. 2015; Corsaro et al. 2017).

131 Forty-five eruptive events characterized by brief but powerful strombolian, lava fountain, and effusive
132 phases, named paroxysms, caused the growth of the NSEC cone (up to a height of about 200 m), and
133 formed compound lava flow fields in VdB (partially covering the 2008–2009 one) and on the south flank.
134 Lava fountains lasted between 30 minutes and 9 hours while concurrent flows were active for up to 12
135 hours. Frequent eruptive events alternated with pauses of several months. Twenty-five, thirteen and six
136 paroxysms occurred from January 2011–April 2012, February–April 2013 and October–December 2013,
137 respectively. Subsequently, only five strombolian and effusive events, lasting from 2 to 67 days, occurred
138 from vents on NSEC flanks and rims up to August 2014. The last paroxysm occurred on 28–29 December
139 2014. Strong strombolian and effusive activity occurred from 31 January–2 February 2015; a fissure on

140 the NSEC north-eastern flank, just below the crater rim, was active from 12–16 May 2015 and three
141 effusive vents on the NSEC high east flank fed single flows from 6–8 December 2015.

142 The VOR, which last erupted in 1999, underwent intense explosive activity from 27 February 2013
143 that lasted, with decreasing intensity, until 17 March. Strombolian activity resumed in late October 2015
144 and increased on 2 December. Four paroxysmal lava fountains occurred from 3–5 December 2015,
145 forming ash plumes up to 14 km high and proximal deposits that filled the crater and overflowed into the
146 adjoining BN. A new sequence of paroxysmal events occurred from 18–25 May 2016, including three
147 lava fountains and intense strombolian activity, the products of which overflowed into the adjoining BN,
148 as well as a small lava flow from a fissure in the saddle between VOR and SEC.

149 The BN, which last erupted in 2002, showed strombolian activity on 11 July 2011 and within a few
150 days formed a lava flow that covered its crater floor. Between July and October 2012, short strombolian
151 episodes built a small cone and new lava flowed onto the crater floor. Vigorous strombolian activity
152 periodically occurred in January–February 2013. Then on 18, 19 and 21 May 2016, the lava erupted from
153 VOR paroxysms overflowed into BN and went on to overflow from its lower western rim, producing
154 three overlapping lava fields on the western flank, towards M. Nunziata, that stopped at 1800 m a.s.l.

155 Small and periodic ash emissions and thermal anomalies have been observed at NEC since 15
156 December 2013. Fissures on NEC eastern flank, from 5 July–10 August 2014, produced strong
157 strombolian activity and lava flows from Valle del Leone (VdL) to the upper VdB, and a lava flow into
158 VdB toward M. Simone on 18–19 May 2016.

160 **Data and methods**

161 A multi-temporal dataset of optical satellite images comprising two stereo-couples acquired in 2012
162 and 2013 from Worldview-2 and Pleiades satellites, respectively, as well as five Pleiades tri-stereo
163 acquisitions between 2015 and 2016 (Table 1), was collected. Pleiades datasets were processed with the
164 OrthoEngine tool implemented in PCI Geomatics software (www.pcigeomatics.com), to extract geocoded
165 DEMs and orthophotos (UTM planimetric datum and ellipsoid, WGS-84, elevations). Image corrections
166 were applied using the rational polynomial functions model based on the Rational Polynomial
167 Coefficients (RPCs), delivered as image metadata, that provide a compact representation of a ground-to-
168 image geometry without the need to measure 3-D GCPs (Fraser 2006). However, to increase the accuracy
169 of DEM georeferencing, the initial RCP functions can be refined by using GCPs measured on the ground
170 or on reference maps. Here, we measured the coordinates of 45 GCPs on Etna's orthophotos (GSDs of
171 0.25 m) and DEMs (1×1 m grid) obtained in 2005 with the airborne High-Resolution Stereo Camera
172 (HRSC-AX) sensor and photogrammetric processing system (Gwinner et al. 2006). Automatic DEM
173 extraction from the Pleiades datasets was based on the Semi-Global Matching method which is
174 particularly efficient in low contrast areas (Eisank et al. 2015). The use of the same GCPs for all Pleiades

175 datasets guarantees co-registration between the various DEMs and therefore the repeatability of
176 measurements from multi-temporal comparisons. An overall accuracy of greater than 0.6 m (Fig. 3) was
177 obtained for both the horizontal and vertical components by analysing the discrepancy between the
178 coordinates of 11 additional Check Points (CPs) measured on the 2005 datasets and on the Pleiades
179 models. Therefore, the final GSD for Pleiades DEMs and orthophotos was set to 1 m and 0.5 m,
180 respectively. Automatic processing of the 2012 Worldview-2 stereo-couple failed owing to the presence
181 of clouds and a volcanic plume, so the data were processed through a manual photogrammetric restitution
182 with the Helava software (Baldi et al. 2005), to extract the DEM of the NSEC area. A DEM acquired in
183 August 2007 (10×10 m grid, UTM planimetric datum and geoid elevations), with the airborne High-
184 Resolution Stereo Camera (HRSC-AX) sensor and photogrammetric processing system (Gwinner et al.
185 2006) to update the topography of Etna's summit area, was also analysed because it represents the
186 topographic surface before the 2007–2016 eruptive activity.

187 The topographic approach was applied to the multi-temporal dataset to quantify the bulk volumes of
188 lava and proximal pyroclastic deposits and estimate the associated precisions. The quality of the DEMs
189 and orthophotos, as well as the image noise due to the presence of clouds and/or volcanic plume were
190 considered, along with the chronology of the eruptive events (Fig. 2), when selecting which satellite
191 datasets to use (Table 2). For example, the October 2015 dataset was excluded owing to clouds in the
192 crater area and because no eruptive events had occurred between this dataset and the previous one
193 (September 2015, with minor plume coverage). Prior to evaluate elevation differences (residuals) between
194 the satellites and the 2007 data (GSDs of 1 m and 10 m, respectively) satellite DEMs were resampled to
195 10 m. However, pairs composed of two satellite DEMs were compared at their original GSD. A number
196 of check areas ($500 \times 500 \text{ m}^2$) that should not have changed between subsequent datasets and that covered
197 different slopes, were defined around Etna's summit and around the 2008–2016 lava flow fields (Fig. 4 a–
198 d). The elevation residuals, measured inside each check area, showed Gaussian distributions for all the
199 DEM pairs. Average residuals and standard deviations from -1.2 to -0.1 m and from 2.6 to 5.3 m,
200 respectively were obtained for pairs composed by two satellite DEMs (Fig. 4 e–g and Table 3). Average
201 residuals of 41.9–43.7 m (due to the different altimetry references) and standard deviations of 2.3–4.3 m,
202 were obtained for the pairs having the 2007 DEM as pre-event surface. To co-register DEMs in individual
203 pairs, the average residuals have been subtracted from the elevations of each resampled Pleiades DEM,
204 obtaining corrected residuals with average check values of around zero (Table 4). The overall quality of
205 the datasets (2007–2016 DEMs) is summarized in Fig. 4h that shows the distributions of the elevation
206 residuals estimated for all the check areas.

207 Before quantifying the new volcanic products, a further check based on an analysis of the orthophotos
208 and shaded relief maps was applied for removing, from the selected DEMs, the values corresponding to
209 artefacts due to volcanic plume and/or clouds in the satellite images. A natural neighbours interpolation

210 was then performed for filling the gaps created during the artefact removal. Post-event orthophotos were
 211 analysed for manually delineating the lava fields, the base of the NSEC cone and the VOR pyroclastic
 212 proximal deposits. Delineation of the lava fields and VOR deposits was verified by checking elevation
 213 differences. The NSEC cone base was checked on post-event slopes from the resampled satellite DEMs,
 214 which highlight the abrupt slope changes at the transition from steep cone sides to the gentler sloping
 215 areas around it. The polygons of the volcanic products were then used to extract, for each DEM pair, a
 216 number of rasters representing the thickness of the different lava fields, the NSEC cone and the VOR
 217 proximal deposits. For each raster, the covered area was determined by multiplying the area of a cell by
 218 the number of pixels, while the bulk volume was measured by summing the products of cell area and
 219 interpolated thickness. The volume standard deviations (σ_V) were calculated from the variance
 220 propagation law (Coltelli et al. 2007):

$$\sigma_V = \sqrt{\sum_{ij} (\Delta x^4 \cdot \sigma_{\Delta z}^2 + 4 \cdot \Delta z_{ij}^2 \cdot \Delta x^2 \cdot \sigma_{\Delta x}^2)}$$

221 where $\sigma_{\Delta x}$ and $\sigma_{\Delta z}$ are the planimetric and vertical accuracies set equal to the DEM GSD and to the
 222 standard deviations of check residuals. For each lava field we also measured the average and maximum
 223 thicknesses as well as the maximum length. For the NSEC cone we also quantified the maximum height
 224 and maximum elevation above sea level (a.s.l.).

225 Since the time intervals covered by Pleiades pairs have durations of ~2–24 months, the analysed DEM
 226 pairs cover from one to fifteen different eruptive events, separated by pauses lasting from few hours up to
 227 ten months. Pairs E and F were the only ones that enabled mapping of individual effusive events
 228 producing single lava flows into the VdB (Table 2). Therefore, we generally measured cumulative
 229 volumes for both the lava fields and the proximal deposits and we divided these quantities by the
 230 corresponding cumulative durations of all the effusive/explosive events (occurred between the two
 231 analysed DEMs) to obtain multi-event eruption rates (mER) and multi-event Deposition Rates (mDR). A
 232 multi-event rate can be seen as the average value of the mean output rate (final volume divided by the
 233 total duration of an event, Harris et al. 2007) for all the single-events occurred between two surveys. This
 234 quantity has the disadvantage of smoothing the differences between the various events, nevertheless, it is
 235 the only output rate that can be evaluated in a posteriori analysis of a series of past eruptions, thus it still
 236 furnishes data useful for investigating the volcano behaviour.

237 Bulk volumes of lava flow fields and proximal deposits (NSEC cone and VOR) were converted to
 238 Dense Rock Equivalent (DRE) to take into account the variable vesicularity of effusive and explosive
 239 products by using average porosities of 20% and 50%, respectively (Andronico et al. 2018). It is not easy
 240 to estimate the porosity of proximal deposits inside VOR, and the actual value could be lower and closer
 241 to that of lava flows. The DRE volumes of distal tephra deposited during all paroxysmal events between
 242 each DEM pair, were then estimated as 4% of the total erupted magma, on the basis of the relative

percentages of lava and tephra assessed for the 25–26 October 2013 Etnean lava fountain (Andronico et al. 2018). The sum of volumes measured for lava and proximal deposits and those estimated for distal deposits gave the total DRE volume of erupted magma. The magma output rate was evaluated by dividing the volume emplaced between two surveys for the corresponding time span, while the average output rate was estimated by considering the total volume over the entire investigated time period.

Results

Geometry and rate of emplacement of the lava fields

We measured the bulk volumes and multi-event eruption rates of Etna lava fields emplaced during a series of eruptive events occurred from May 2008 to May 2016 (Table 5 and Fig. 5). Volumes of the same order of magnitude were erupted during the 2008–2009 eruption and the first thirty-eight NSEC paroxysms, lasting in total ~420 d and ~2.3 d, respectively. The following fifteen events erupted about half of that volume. Finally, single effusive events and BN overflows erupted quite low lava volumes.

Events that were mainly effusive had eruption rates ranging between ~2 m³/s (2008–2009) and ~14 m³/s (6–8 December 2015). Periods containing several paroxysms presented mER as high as ~398 m³/s (January 2011–April 2013). When the lava flow fields were produced by both long-lasting effusive events and short-lasting paroxysms the estimated mER were quite low, ~4 m³/s and ~11 m³/s for 15 events (October 2013–May 2015) and 53 events (January 2011–September 2015), respectively. Finally, overflows from summit craters concurrent with paroxysmal activity (May 2016) had an intermediate mER≅71 m³/s.

Distribution and rate of emplacement of the proximal deposits

The proximal pyroclastic deposits of 45 paroxysmal events, between 2011 and 2015, led to the growth of the NSEC cone to ~46 × 10⁶ m³, over a total duration of ~4 d (mDR≅137 m³/s). About half of the pyroclastic deposits accumulated during the first 25 paroxysms (2011–2012) over total duration of ~50 h (mDR≅117 m³/s). Thirteen more paroxysms before April 2013, over a total duration of ~12 h, added ~10 × 10⁶ m³ (mDR≅240 m³/s). Finally, the last seven paroxysms added ~15 × 10⁶ m³, over a total duration of ~31 h (mDR≅129 m³/s). After September 2015, one strombolian and effusive event at NSEC produced minor growth of the cone (~0.3 × 10⁶ m³). The cone height rapidly increased to ~160 m during the first 25 paroxysms, then slower growth led, in 22 more paroxysms, to a maximum height of ~200 m corresponding to the maximum elevation of 3287 m a.s.l. (Table 6 and Fig. 6).

Approximately 6.1 and 8.4 × 10⁶ m³ of pyroclastic deposits accumulated inside the VOR and BN crater depressions during the four VOR paroxysms of December 2015 and all seven VOR paroxysms, having total durations of ~5 h and ~15 h, respectively (mDR≅339 m³/s and mDR≅43 m³/s). During the May 2016 paroxysms the lava erupted from VOR filled the crater depression, partially occupied by the

277 December 2015 deposits, and overflowed from BN (measured bulk volume $\sim 3 \times 10^6 \text{ m}^3$), thus the DRE
278 magma volume is $\sim 3.4 \times 10^6 \text{ m}^3$, corresponding to a magma output rate of $\sim 100 \text{ m}^3/\text{s}$ (Table 6 and Fig. 6).

279 Volume of erupted magma

280 We measured the DRE volumes of erupted magma by considering the effusive and explosive
281 products, both distal and proximal (Fig. 7). The values obtained are $\sim 57 \times 10^6 \text{ m}^3$ for the 2008–2009
282 effusive eruption, $\sim 114 \times 10^6 \text{ m}^3$ for the 38 paroxysms of January 2011–April 2013, $\sim 62 \times 10^6 \text{ m}^3$ for the
283 15 events of October 2013–May 2015, $\sim 9 \times 10^6 \text{ m}^3$ for the five events of May–December 2015 and $\sim 6 \times$
284 10^6 m^3 for the four events of December 2015–May 2016. Over the full 8-year time period investigated
285 (May 2008 to May 2016) we measured a DRE volume of erupted magma equal to $248.4 \pm 2.1 \times 10^6 \text{ m}^3$
286 (about 76% of this volume is related to lava fields). This corresponds to a multi-event eruption rate (total
287 volume/total duration) of $5.53 \text{ m}^3/\text{s}$, over $\sim 520 \text{ d}$ of total duration of the eruptions, and to an average
288 output rate of $0.98 \text{ m}^3/\text{s}$, over the 8 years.

290 Discussion

291 Measurements of the erupted products and of the magma output rate at active volcanoes are
292 important both for monitoring the eruption development and quantifying the associated hazard and
293 because they provide important data for modelling the magma dynamics driving an eruption. Current
294 time-averaged eruption rates can be compared to past measurements giving insight into long-term trends
295 in volcanic behaviour (e.g. Wadge, 1981; Kubanek et al. 2017; Bonny et al. 2018).

296 The results obtained in this work can be compared with previously published volumes of lava flows
297 and pyroclastic deposits and magma output rates. Our volume estimates for the 2008–2009 and 2011–
298 2015 lava flow fields showed a minimal discrepancy of 3–4 % with those obtained applying the
299 topographic approach to DEMs (1 m GSD) extracted on 2007 and 2010 from aerial LIDAR surveys
300 (Behncke et al. 2016) and from a subset of our data, that is the 2005 aerophotogrammetric and the 18
301 December 2015 Pleiades DEMs (4 m GSD, Ganci et al. 2018). However, the volume comparisons for the
302 NSEC and the VOR pyroclastic deposits obtained, respectively, with a Pleiades dataset (Ganci et al.
303 2018) and a combination of DEMs from a 2010 aerial LIDAR and photogrammetric helicopter surveys
304 performed on December 2015 (1 m GSD, Neri et al. 2017), showed a larger discrepancy of $\sim 19\%$. The
305 dissimilarities for the NSEC are due to a different delimitation of the volcanic products and different pre-
306 event DEMs, which can result in including products from previous volcanic activities. The difference for
307 VOR could be due to plume from the summit craters that resulted in elevation outliers on Pleiades DEMs.
308 Comparing our results with previously published works based on the measurement of flow area and
309 thickness (planimetric approach), performed for most of the eruptive episodes, shows that values from the
310 literature are underestimated. In particular, the lava volumes accumulated in the 38 NSEC paroxysms of
311 2011–2013, the 15 events of 2013–2015, the 53 events of January 2011–May 2015 and the 6–8 December

312 2015 effusive event are underestimated by ~47%, ~15%, ~35% and ~6%, respectively (Behncke et al.
313 2014; De Beni et al. 2015; Corsaro et al. 2017). The higher discrepancies obtained when considering
314 more events derive from the error propagation during the summation of multiple volumes. Moreover, for
315 compound lava fields formed during frequently repeated eruptive events, higher discrepancies are due to
316 the difficulty of estimating the mean lava thickness for an irregular morphology. Therefore, the
317 planimetric approach can be applied for rapid preliminary quantification of the area and volume of simple
318 lava flows. However, DEMs and orthophotos from high-resolution satellite stereo-pairs can effectively
319 support the topographic approach which is more reliable when dealing with compound lava flows and
320 wide morphological variations, such as the growth of a new pyroclastic cone

321 Our results can be compared with the average values of previously published lava volumes, evaluated
322 from thermal satellite data. These volumes are always given as ranges owing to the large and unavoidable
323 uncertainty of the underlying assumptions used for converting the measured radiance to time-averaged
324 discharge rates (TADR). The TADR estimates can also be influenced by the presence of an ash column
325 that attenuates or obscures the thermal anomaly (Ganci et al. 2012). Our measures, compared with the
326 corresponding average volumes from thermal data, are higher by ~35% (Ganci et al. 2012) and ~5%
327 (Harris et al. 2011) for the 2008–2009 eruption; and by ~16% for the 2011–2015 lava fields (Ganci et al.
328 2018). Our measures approximately correspond to the upper limit of the variability range of volumes
329 from thermal data.

330 By analysing the overall results, we measured a total DRE volume of $\sim 248 \times 10^6 \text{ m}^3$ ($\sim 190 \times 10^6 \text{ m}^3$
331 from lava fields), which corresponds to a multi-event eruption rate of $5.53 \text{ m}^3/\text{s}$ for 520 days of eruptive
332 activity and to an average output rate of $\sim 0.98 \text{ m}^3/\text{s}$ over eight years. Over ten years, this would result in a
333 total DRE volume of $\sim 310 \times 10^6 \text{ m}^3$. These values are in accordance with the erupted lava volumes of
334 $\sim 300 \times 10^6 \text{ m}^3$ and mean output rate of $0.6\text{--}0.9 \text{ m}^3/\text{s}$ obtained, on a decadal scale, analysing Etna's 1980–
335 2010 effusive activity from thermal satellite data and with the 2001–2010 mean output rate of $0.97\text{--}1.07$
336 m^3/s obtained by including tephra volumes from the literature (Harris et al. 2011). Our average output rate
337 is ~20% higher than the value expected for the 1993–2013 Etna activity, analysed by combining volumes
338 from the literature measured with different techniques, including analysis of satellite thermal data and the
339 planimetric approach applied to the thirty-eight 2011–2013 fountains (Bonaccorso and Calvari 2013).

340 By analysing the output rates we measured over the different time intervals, we observed that a
341 greater magma output ($\sim 1.6 \text{ m}^3/\text{s}$) is associated with long-lasting lateral effusive eruptions (2008–2009).
342 An output rate of $\sim 1 \text{ m}^3/\text{s}$ was measured for the subsequent two periods (up to May 2013 and May 2013–
343 May 2015) mostly characterized by short-lasting paroxysms interspersed with pauses lasting from a few
344 hours to ~10 months. Finally, a lower output rate ($\sim 0.4\text{--}0.5 \text{ m}^3/\text{s}$) was found during two time periods
345 (May–December 2015 and December 2015–May 2016) characterized by brief effusive events and very
346 short paroxysms separated by pauses of a few months. Even though the eruption rate associated with each

347 paroxysm is quite high (some hundreds of m^3/s) it appears to be insufficient to discharge all the
348 accumulated magma and a series of repeated events can occur in very short time.

350 **Conclusions**

351 This work quantified the lava and the pyroclastic (proximal and distal) products erupted at Etna over
352 an 8-year period (2008–2016), characterized by simultaneous intense explosive and effusive activity, and
353 evaluated the corresponding magma average output rate, thus obtaining data useful for analysing the long-
354 term Etna discharge rate. Although previous research exists which quantifies Etna's recent eruptive
355 activity using different techniques, we applied one methodology to a homogeneous and comprehensive
356 dataset to quantify the DRE magma volumes and the output rate. In particular, we quantified the lava and
357 proximal products, and associated uncertainties, applying the topographic approach to a time-series of co-
358 registered DEMs and orthophotos (with 1- and 0.5-m-pixel resolutions respectively), extracted from six
359 specifically tasked Pleiades tri-stereo pairs (with time intervals of ~2–24 months) plus one
360 aerophotogrammetric DEM (10 m pixel resolution), used as reference topographic surface. Maximum
361 percentage errors of ~3.4 and ~4.2% were obtained for the volumes of the lava fields and the NSEC cone,
362 respectively. We then estimated the distal products by applying the percentages of lava and tephra erupted
363 at the same time, which have been accurately quantified for the 25–26 October 2013 lava fountain of Etna
364 in a previous research.

365 The performed analysis showed that specifically tasked optical images, acquired from meter-
366 resolution satellite systems capable of daily revisits to any point on the globe, are key data for monitoring
367 an active volcano. Such data enable a swift response to an eruptive crisis allowing a rapid, complete and
368 accurate quantification of the volcanic products and of the related hazard, as well as the updating of
369 topographic data. Above all, such data allow monitoring of the volcanic activity to be carried out without
370 putting personnel at risk. Therefore, if it would be possible to task Pleiades acquisitions to systematically
371 monitoring long-lasting eruptions, the collected data could be used to improve inventories of magma
372 output rate thus supporting both the hazard assessment analysis and the understanding of system
373 dynamics (c.f. Wadge, 1981).

374 Our study was here successfully applied to a well-monitored volcano: Etna. The Pleiades global
375 coverage and the theoretical possibility of daily tasking data acquisition, on user-specified areas, enable
376 this methodology to be applied to the monitoring of remote or hazardous volcanoes that may be difficult
377 to access for repeat field surveys.

379 **Acknowledgements**

380 We acknowledge Pierre Briole and Marcello de Michele for providing Pleiades data, analysed in this
381 work, through the Space Volcano Observatory sur Pleiades (SVOP) project

(http://volcano.terre.fr/svo_projects). We are grateful to Massimo Fabris for processing the Worldview 2012 data to extract the DEM of the NSEC cone. We are grateful to Eisuke Fujita, an anonymous reviewer and the associate editor, Michael R. James, for their comments and feedback which greatly improved this manuscript and to William Moreland for improving the English.

References

Andronico D, Behncke B, De Beni E, Cristaldi A, Scollo S, Lopez M, Lo Castro MD (2018) Magma Budget From Lava and Tephra Volumes Erupted During the 25-26 October 2013 Lava Fountain at Mt Etna. *Front. Earth. Sci.* 6, 116. <https://doi.org/10.3389/feart.2018.00116>

Baldi P, Fabris M, Marsella M, Monticelli R (2005) Monitoring the morphological evolution of the Sciara del Fuoco during the 2002–2003 Stromboli eruption using multi-temporal photogrammetry. *ISPRS Journal of Photogrammetry and Remote Sensing* 59:199–211

Bagnardi M, González PJ, Hooper A (2016) High-resolution digital elevation model from tri-stereo Pleiades satellite imagery for lava flow volume estimates at Fogo Volcano. *Geophys Res Lett* 43:6267–6275. <https://doi.org/10.1002/2016GL069457>

Behncke B, Branca S, Corsaro RA, De Beni E, Miraglia L, Proietti C (2014) The 2011–2012 summit activity of Mount Etna: birth, growth and products of the new SE crater. *J Volcanol Geoth Res* 270:10–21. <https://doi.org/10.1016/j.jvolgeores.2013.11.012>

Behncke B, Fornaciai A, Neri M, Favalli M, Ganci G, Mazzarini F (2016) Lidar surveys reveal eruptive volumes and rates at Etna, 2007–2010. *Geophys Res Lett* 43:4270–4278. <https://doi.org/10.1002/2016GL068495>

Boissin MB, Gleyzes A, Tinel C (2012) The Pleiades System and Data Distribution. In: *IEEE International Geoscience and Remote Sensing Symposium, Munich, Germany*, pp 7098–7101

Bonaccorso A and Calvari S (2013) Major effusive eruptions and recent lava fountains: Balance between expected and erupted magma volumes at Etna volcano. *Geophys Res Lett* 40:6069–6073. <https://doi.org/10.1002/2013GL058291>

Bonny E, Thordarson T, Wright R, Höskuldsson A, Jónsdóttir I (2018) The volume of lava erupted during the 2014 to 2015 eruption at Holuhraun, Iceland: A comparison between satellite- and ground-based measurements. *J Geophys Res: Solid Earth* 123:5412–5426. <https://doi.org/10.1029/2017JB015008>

Calvari S, Coltelli M, Neri M, Pompilio M, Scrivano V (1994) The 1991-1993 Etna eruption: Chronology and lava flow-field evolution. *Acta Volcanol* 4:1–14

Coltelli M, Proietti C, Branca S, Marsella M, Andronico D, Lodato L (2007) Analysis of the 2001 lava flow eruption of Mt. Etna from three-dimensional mapping. *J Geophys Res* 112, F02029. <https://doi.org/10.1029/2006JF000598>

417 Coltelli M, D'Aranno PJV, De Bonis R, Guerrero F, Marsella M, Nardinocchi C, Pecora E, Proietti C,
418 Scifoni S, Scutti M, Wahbeh W (2017) The use of surveillance cameras for the rapid mapping of lava
419 flow: an application to Mount Etna Volcano. *Remote Sens* 9, 192. <https://doi.org/10.3390/rs9030192>

420 Corsaro RA, Andronico D, Behncke B, Branca S, De Beni E, Caltabiano T, Ciancitto F, Cristaldi A,
421 De Beni E, La Spina A, Lodato L, Miraglia L, Neri M, Salerno G, Scollo S, Spata G (2017) Monitoring
422 the December 2015 summit eruptions of Mt. Etna (Italy): implications on eruptive dynamics. *J Volcanol*
423 *Geoth Res* 341: 53–69. <https://doi.org/10.1016/j.jvolgeores.2017.04.018>

424 De Beni E, Behncke B, Branca S, Nicolosi I, Carluccio R, D'Ajello Caracciolo F, Chiappini M (2015)
425 The continuing story of Etna's New Southeast Crater (2012–2014): evolution and volume calculations
426 based on field surveys and aerophotogrammetry. *J Volcanol Geoth Res* 303:175–186.
427 <https://doi.org/10.1016/j.jvolgeores.2015.07.021>

428 Dvigalo V, Shevchenko A, Svirid I (2016) Photogrammetric Survey in Volcanology: A Case Study for
429 Kamchatka Active Volcanoes. In: Nemeth K (ed) *Updates in Volcanology - From Volcano Modelling to*
430 *Volcano Geology*, InTech, pp 55–79. <https://doi.org/10.5772/63577>

431 Eisank C, Rieg L, Klug C, Kleindienst H (2015) Semi-Global Matching of Pleiades Tri-Stereo
432 Imagery to Generate Detailed Digital Topography for High-Alpine Regions. *GI_Forum – Journal for*
433 *Geographic Information Science* 3:168–177. <https://doi.org/10.1553/giscience2015s168>

434 Francis P, Rothery D (2000) Remote sensing of active volcanoes. *Annu. Rev. Earth Planet. Sci.* 28:81–
435 106

436 Fraser CS, Dial G, Grodecki J (2006) Sensor orientation via RPCs. *ISPRS Journal of Photogrammetry*
437 *and Remote Sensing* 60, 3:182–194

438 Ganci G, Vicari A, Cappello A, Del Negro C (2012) An emergent strategy for volcano hazard
439 assessment: From thermal satellite monitoring to lava flow modelling. *Remote Sensing of Environment*,
440 119:197–207

441 Ganci G, Cappello A, Bilotta G, Herault A, Zago V, Del Negro C (2018) Mapping Volcanic Deposits
442 of the 2011–2015 Etna Eruptive Events Using Satellite Remote Sensing. *Front. Earth Sci.* 6, 83.
443 <https://doi.org/10.3389/feart.2018.00083>

444 Gwinner K, Coltelli M, Flohrer J, Jaumann R, Matz KD, Marsella M, Roatsch T, Scholten F, Trauthan
445 F (2006) The HRSC-AX Mt. Etna project: high-resolution orthoimages and 1 m DEM at regional scale.
446 In: *Proceedings ISPRS Archives* 23, 1, *From Sensors to Imagery* (Paris, 4–6 July 2006), 6 pp, T05-23

447 Harris AJL, Dehn J, Calvari S (2007) Lava effusion rate definition and measurement: a review. *Bull*
448 *Volcanol* 70:1–22. <https://doi.org/10.1007/s00445-007-0120-y>

449 Harris AJL, Steffke A, Calvari S, Spampinato L (2011) Thirty years of satellite-derived lava discharge
450 rates at Etna: Implications for steady volumetric output. *J Geophys Res* 116, B08204.
451 <https://doi.org/10.1029/2011JB008237>

452 Honda K, Nagai M (2002) Real-time volcano activity mapping using ground-based digital imagery.
453 ISPRS Journal of Photogrammetry and Remote Sensing 57:159–168
454 http://volcano.terre.fr/svo_projects. Accessed 18 March 2019

455 Kubanek J, Westerhaus M, Heck B (2017) TanDEM-X Time Series Analysis Reveals Lava Flow
456 Volume and Effusion Rates of the 2012–2013 Tolbachik, Kamchatka Fissure Eruption. *J Geophys Res:*
457 *Solid Earth* 122:7754–7774. <https://doi.org/10.1002/2017JB014309>

458 Marsella M, Proietti C, Sonnessa A, Coltelli M, Tommasi P, Bernardo E (2009) The evolution of the
459 Sciara del Fuoco subaerial slope during the 2007 Stromboli eruption: Relation between deformation
460 processes and effusive activity. *J Volcanol Geotherm Res* 182:201–213

461 Marsella M, Nardinocchi C, Proietti C, Daga L, Coltelli M (2014) Monitoring Active Volcanos Using
462 Aerial Images and the Orthoview Tool. *Remote Sens* 6:12166–12186. <https://doi.org/10.3390/rs61212166>

463 Martino M, Marsella M, Scifoni S, Coltelli M, Proietti C, Chowdhury TA, Minet C, Giannone F (2016)
464 Monitoring an active volcanic area and mapping lava flows with multisource data: The case of Mount
465 Etna from 2011 to 2015. *EEEIC 2016 - International Conference on Environment and Electrical*
466 *Engineering*, 7–10 June 2016. <https://doi.org/10.1109/EEEIC.2016.7555732>

467 Mouginis-Mark PJ, Pieri DC, Francis PW, Wilson L, Self S, Rose WI, Wood CA (1989) Remote
468 sensing of volcanos and volcanic terrains. *EOS Transactions of the American Geophysical Union*
469 70:1567–1575. <https://doi.org/10.1029/89EO00396>

470 Naranjo MF, Ebmeier SK, Vallejo S, Ramón P, Mothes P, Biggs J, Herrera F (2016) Mapping and
471 measuring lava volumes from 2002 to 2009 at El Reventador Volcano, Ecuador, from field measurements
472 and satellite remote sensing. *Journal of Applied Volcanology* 5, 8. [https://doi.org/10.1186/s13617-](https://doi.org/10.1186/s13617-0160048-z)
473 [0160048-z](https://doi.org/10.1186/s13617-0160048-z)

474 Neri M, De Maio M, Crepaldi S, Suozzi E, Lavy M, Marchionatti F, Calvari S, Buongiorno MF (2017)
475 Topographic Maps of Mount Etna’s Summit Craters, updated to December 2015. *Journal of Maps* 13,
476 2:674–683. <https://doi.org/10.1080/17445647.2017.1352041>

477 Rowland S, Harris A, Wooster M, Amelung F, Garbeil H, Wilson L, Mouginis-Mark P (2003)
478 Volumetric characteristics of lava flows from interferometric radar and multispectral satellite data: The
479 1995 Fernandina and 1998 Cerro Azul eruptions in the western Galapagos. *Bull. Volcanol.*, 65:311–330.
480 <https://doi.org/10.1007/s00445-002-0262-x>.

481 Stevens NF, Wadge G, Murray JB (1999) Lava flow volume and morphology from digitised contour
482 maps: A case study at Mount Etna, Sicily. *Geomorphology* 28:251–261

483 Wadge G (1981) The variation of magma discharge during basaltic eruptions. *J. Volcanol. Geothermal*
484 *Res.* 11:139–168
485 www.pcigeomatics.com. Accessed 18 March 2019
486

Date	Satellite	Acquisition mode	Spatial Resolution (m)	% cloud cover	Quality/disturbs	Time interval (days)
07 August 2012	Worldview	Stereo couple	0.5	8	Volcanic plume from the craters and clouds southward of the crater area	-
12 May 2013	Pleiades-1A	Stereo couple	0.5	4	Clouds covering the Valle del Bove	275
05 September 2015	Pleiades-1A	Tristereero	0.5	2	Volcanic plume from the craters	833
07 October 2015	Pleiades-1B	Tristereero	0.5	4	Clouds coverage on the craters	32
18 December 2015	Pleiades-1A	Tristereero	0.5	0	Presence of snow in the north area	71
24 December 2015	Pleiades-1B	Tristereero	0.5	0	Widespread snow	6
18 July 2016	Pleiades-1A	Tristereero	0.5	0	Clean	204

488

Table 1 Multi-temporal satellite datasets used to analyse the morphological evolution of Etna summit area.

489

DEM pair	Pre-event DEM	Post-event DEM	Time interval (days)	Eruptive events from	Eruptive events between the two DEMs	Eruption style
A	August 2007	07 August 2012	~ 1769	SEC	3 paroxysms: 4–5 September 2007, 23–24 November 2007 and 10 May 2008	Explosive and effusive
				Fissure in VdB	2008/09 lateral eruption	Effusive
				NSEC	25 paroxysms between 12 January 2011 and 24-04-2012	Explosive and effusive
B	August 2007	12 May 2013	~ 2071	SEC	3 paroxysms: 4–5 September 2007, 23–24 November 2007 and 10 May 2008	Explosive and effusive
				Fissure in VdB	2008/09 lateral eruption	Effusive
				NSEC	38 paroxysms between 12 January 2011 and 28-04-2013	Explosive and effusive
C	August 2007	05 September 2015	~ 2904	SEC	3 paroxysms: 4–5 September 2007, 23–24 November 2007 and 10 May 2008	Explosive and effusive
				Fissure in VdB	2008/09 lateral eruption	Effusive
				NSEC	47 paroxysms between 12 January 2011 and 31 January 2015	Explosive and effusive
				Fissures on NSEC flanks	5 events between 14 December 2013 and 12 May 2015	Effusive
				Fissure at NEC base	1 event between 05 July 2014 and 10 August 2014	Effusive
D	12 May 2013	05 September 2015	833	NSEC	9 paroxysms between 26 October 2013 and 31 January 2015	Explosive and effusive
				Fissures on NSEC flanks	5 events between 14 December 2013 and 16 May 2015	Effusive
				Fissure at NEC base	1 event between 03 July 2014 and 10 August 2014	Effusive
E	05 September 2015	18 December 2015	103	Fissure on NSEC flanks	1 event on 06–08 December 2015	Effusive
F	18 December 2015	18 July 2016	210	VOR	4 paroxysms on 03–05 December 2015	Explosive
				Fissure at NEC base	1 event on 18–19 May 2016	Effusive
				VOR	3 paroxysms on 18–21 May 2016	Explosive
				BN	3 overflows on 18–21 May 2016	Effusive
G, H	August 2007	18 December 2015, 24 December 2015	~ 3007, ~ 3013	SEC	3 paroxysms: 4–5 September 2007, 23–24 November 2007 and 10 May 2008	Explosive and effusive
				Fissure in VdB	2008/09 lateral eruption	Effusive
				NSEC	47 paroxysms between 12 January 2011 and 31 January 2015	Explosive and effusive
				Fissure at NEC base	1 event between 05 July 2014 and 10 August 2014	Effusive
I	August 2007	18 July 2016	~ 3250	VOR	4 paroxysms on 03–05 December 2015	Explosive
				SEC	3 paroxysms: 4–5 September 2007, 23–24 November 2007 and 10 May 2008	Explosive and effusive
				Fissure in VdB	2008/09 lateral eruption	Effusive
				NSEC	47 paroxysms between 12 January 2011 and 31 January 2015	Explosive and effusive
				Fissure at NEC base	2 events between 05 July 2014 and 10 August 2014 and on 18–19 May 2016	Effusive
				VOR	7 paroxysms: 4 on 03–05 December 2015 and 3 on 18–21 May 2016	Explosive
				BN	3 overflows on 18–21 May 2016	Effusive

Table 2 Selected DEM pairs, events and style of activity covered.

490

491

492

493

DEM pair	Number of check areas	Min res (m)	Max res (m)	Aver res (m)	Stand dev (m)
D	7	-115.5	59.1	-1.2	5.3
E	4	-42.7	40.4	-0.1	2.9
F	7	-40.6	52.8	-0.5	2.6

Table 3 Check area statistics for Pleiades DEM pairs.

DEM pair	Min res (m)	Max res (m)	Aver res (m)	Stand dev (m)	Min corrected res (m)	Max corrected res (m)	Aver corrected res (m)
A	22.2	57.6	41.9	2.3	-19.7	15.7	0.01
B	19.7	67.9	43.7	2.8	-24.0	24.2	-3.4 x 10 ⁻⁶
C	-22.5	82.0	43.1	4.3	-65.6	39.0	1.9 x 10 ⁻⁶
G	8.1	71.1	42.7	3.4	-34.5	28.5	-3.0 x 10 ⁻⁶
H	26.8	67.9	43.4	3.1	-16.6	24.5	1.2 x 10 ⁻⁷
I	31.1	53.9	42.2	2.3	-11.1	11.7	-3.5 x 10 ⁻⁶

Table 4 Check area statistics for satellite-2007 DEM pairs. Last three columns: statistics after subtracting the average residual.

DEM pair	Measured products	Not-measured products	Effusion duration (d)	Max L (km)	Max T (m)	Aver T (m)	A (10 ⁶ m ²)	V (10 ⁶ m ³)	σ _v (10 ⁶ m ³)	ER*/mER (m ³ /s)
B	Compound lava field in VdB from the 2008–2009 effusive eruption and 10 May 2008 SEC paroxysm	Compound lava field in VdB from 38 NSEC paroxysms owing to clouds in the post-events dataset	420.0	6.4	82.4	13.15	5.4	71.6	0.9	2.0*
C-D	Compound lava field in VdB from 38 NSEC paroxysms (January 2011–April 2013)		2.3	-	-	-	-	79.8	1.6	398.4
D	Compound lava fields in VdB and on the S flank from 14 NSEC events (7 paroxysms) and 1 from NEC base (October 2013–May 2015) South lava field in VdB estimated through the planimetric approach owing to clouds in the pre-event dataset	1-km-long simple flow to the NE of NSEC owing to plume in the post-eruption orthophoto	125.8	4.5	44.0	6.9	6.8	46.4	1.6	4.3
C	Compound lava field in VdB from 52 NSEC events (47 paroxysms) and 1 from NEC base (January 2011–May 2015)		128.1	4.5	99.9	15.4	8.1	126.1	1.2	11.4
E	3 simple flows in VdB from 1 event from NSEC flank (6–8 December 2015)		2.0	3.8	24.7	4.6	0.5	2.432	0.009	14.1*
F	Simple flow in VdB from 1 event at NEC base (18–21 May 2016) Compound field on the W flank from 3 events from BN (18–21 May 2016)		0.4	2.5	23.3	1.7	0.2	0.376	0.002	10.4*
			0.5	3.1	18.5	3.1	0.9	2.809	0.008	70.7

Table 5 Quantification of effusive products covered by DEM pairs: maximum length of flow fields (L), thicknesses (T), area (A), total bulk volume and standard deviation (V and σ_v).

DEM pair	Analysed crater	Date of last event	Cumulative number of paroxysms	Cumulated fountain duration (d)	A (10 ⁶ m ²)	Max H (m)	Max Elev (m a.s.l.)	Cumulative V (10 ⁶ m ³)	σ _v (10 ⁶ m ³)	mDR (m ³ /s)
A	NSEC	23 April 2012	25	2.1	0.4	162	3225	21.2	0.9	117
B	NSEC	28 April 2013	38	2.6	0.5	174	3275	31.4	1.1	240
C	NSEC	16 May 2015	47	3.1	0.6	183	3287	45.9	1.4	129
H	NSEC	08 December 2015	47	3.1	0.6	198	3287	46.2	1.4	0
E, H	VOR	05 December 2015	4	0.2	0.5	-	-	6.07	0.03	336
I	VOR	21 May 2016	7	0.6	0.3	-	-	8.35	0.03	448

Table 6 Quantification of NSEC and VOR proximal deposits: area (A), maximum height and elevation (H and Elev), bulk volume and standard deviation (V and σ_v).

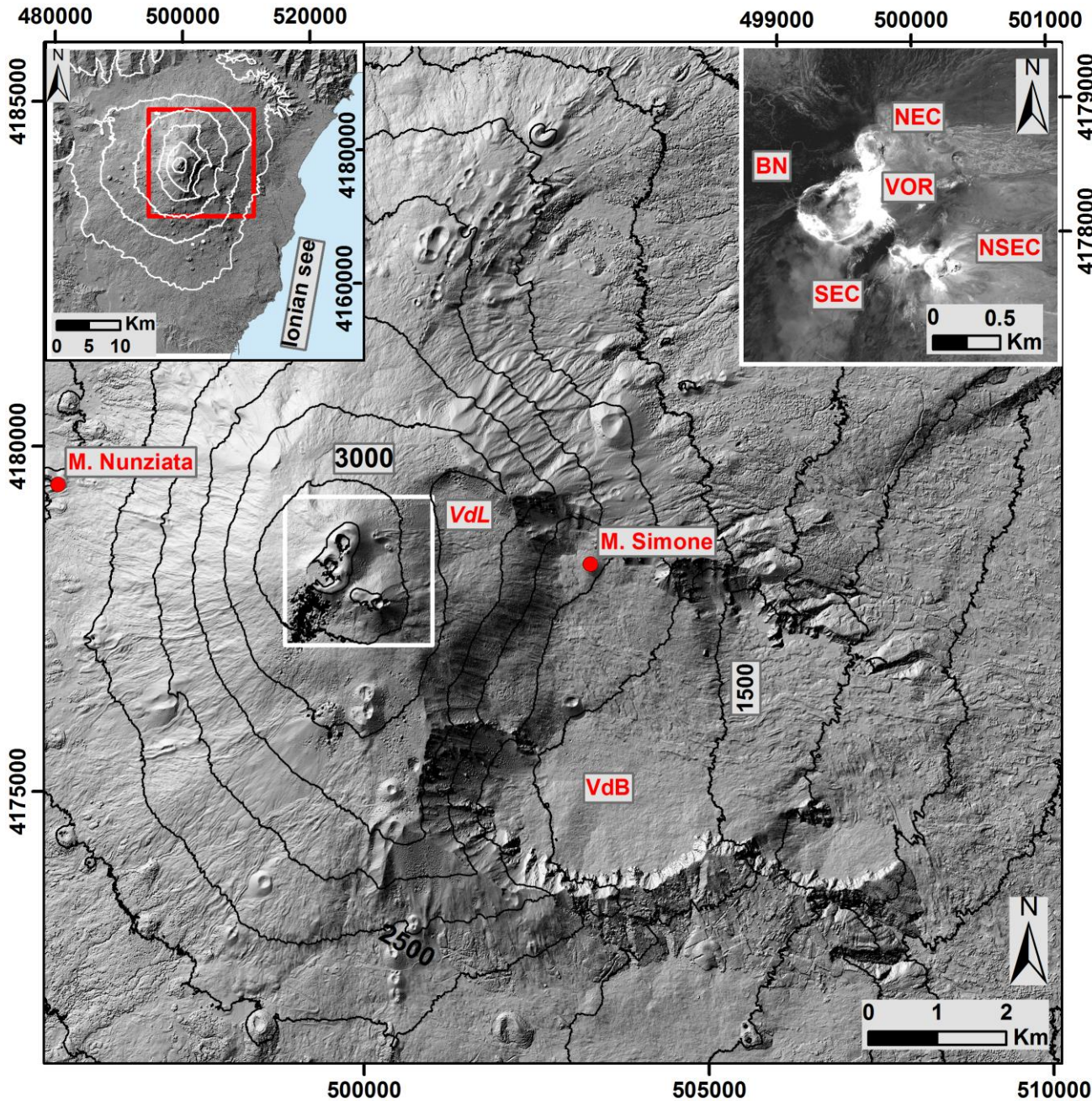
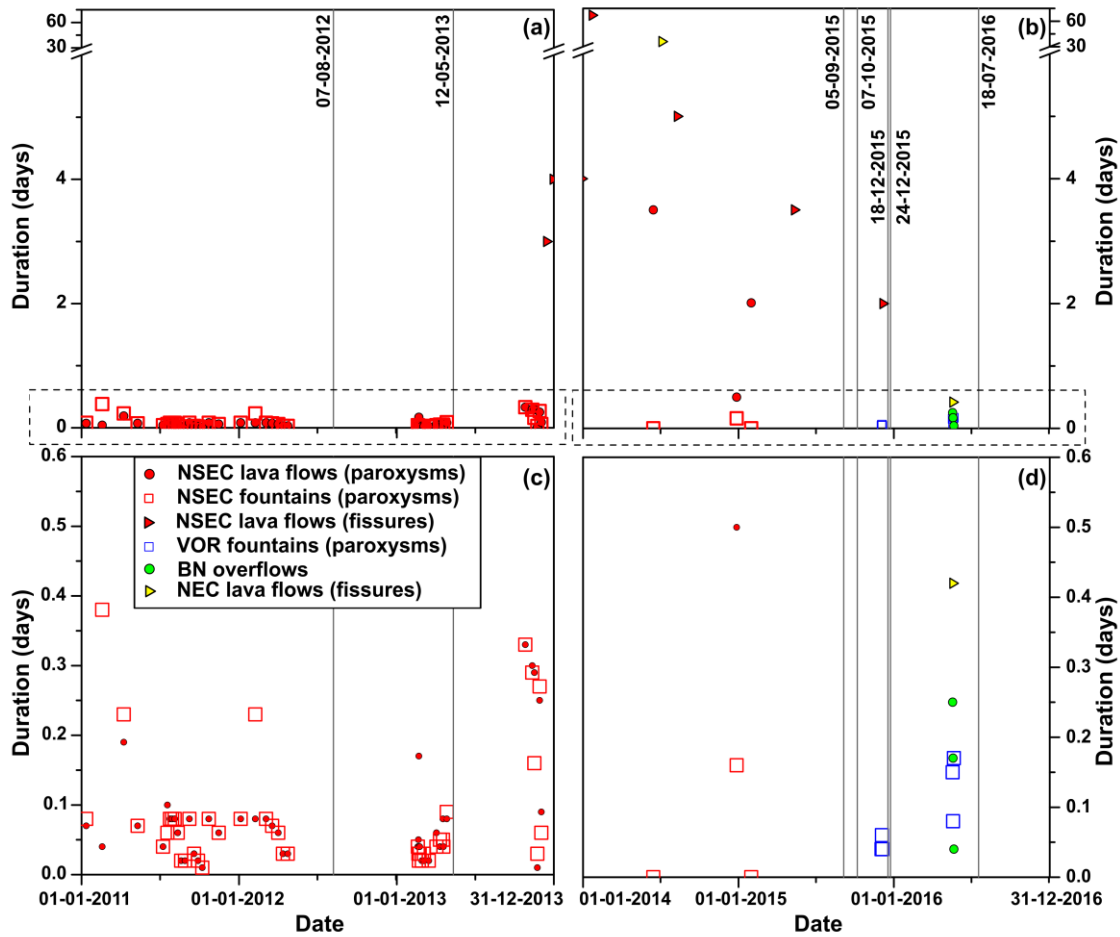
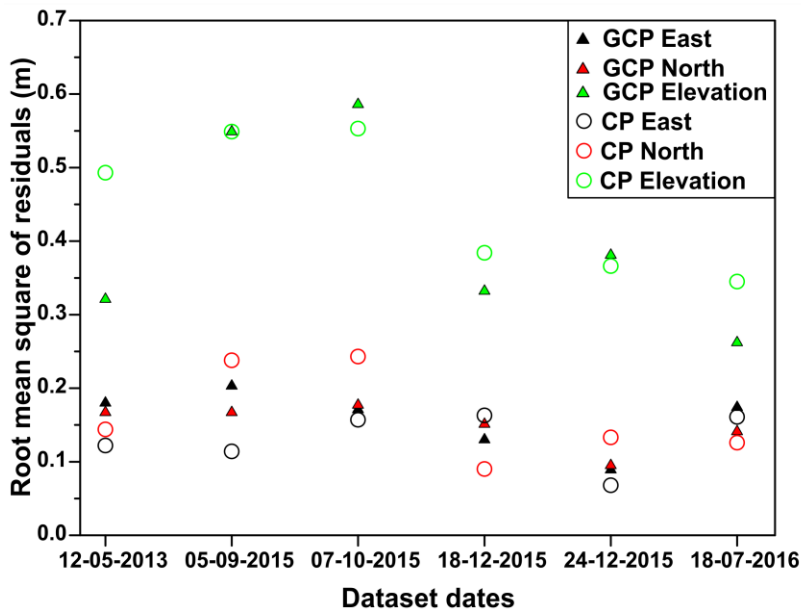


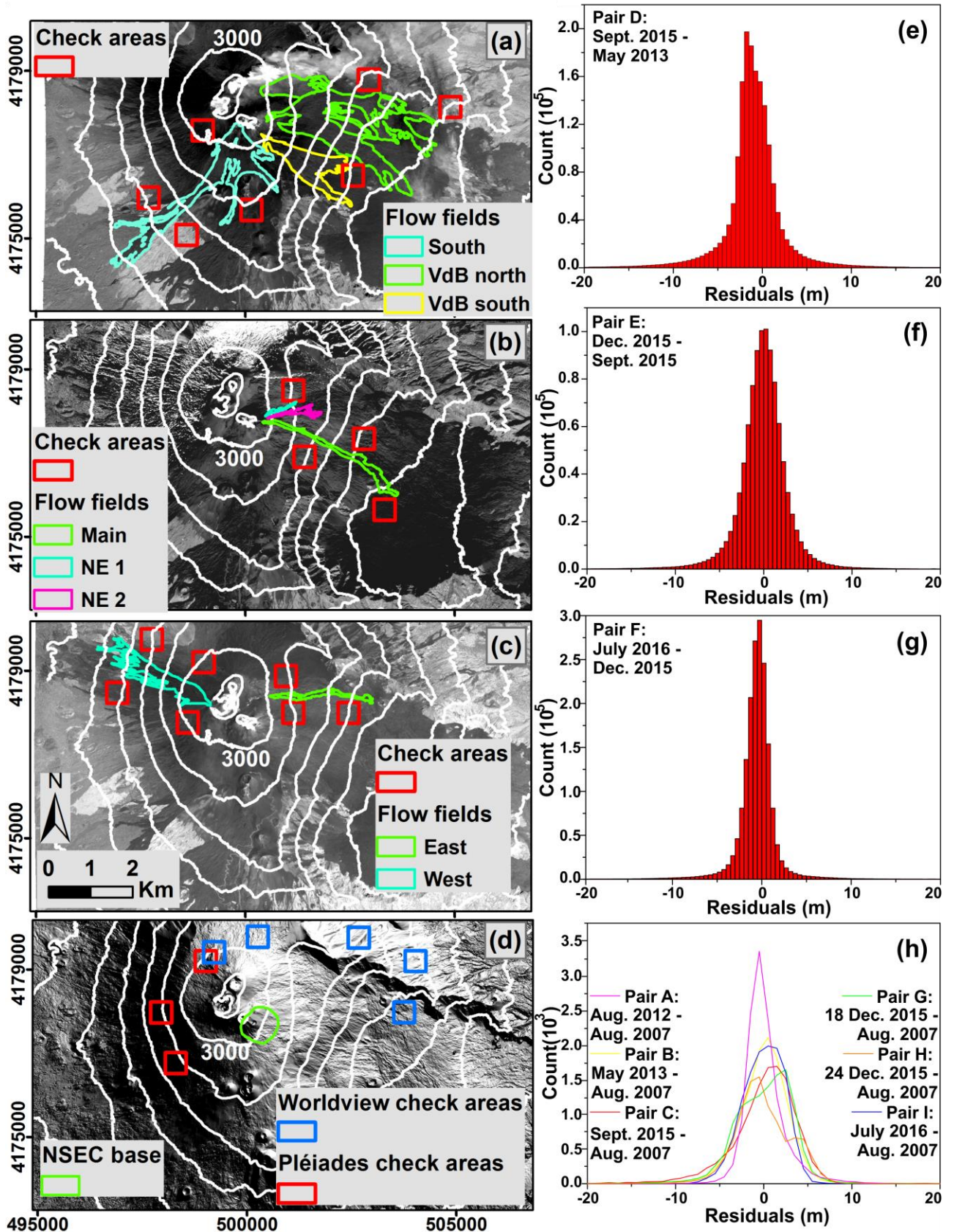
Fig. 1 Shaded relief of the 18 July 2016 Pleiades DEM with contour lines of height above the geoid every 250 m. Right inset shows Etna summit area (white square) from the 18 July 2016 orthophoto. Left inset locates the investigated area (red square) on the 2005 Etna shaded relief (Gwinner et al. 2006) with contour lines of geoid height every 500 m.



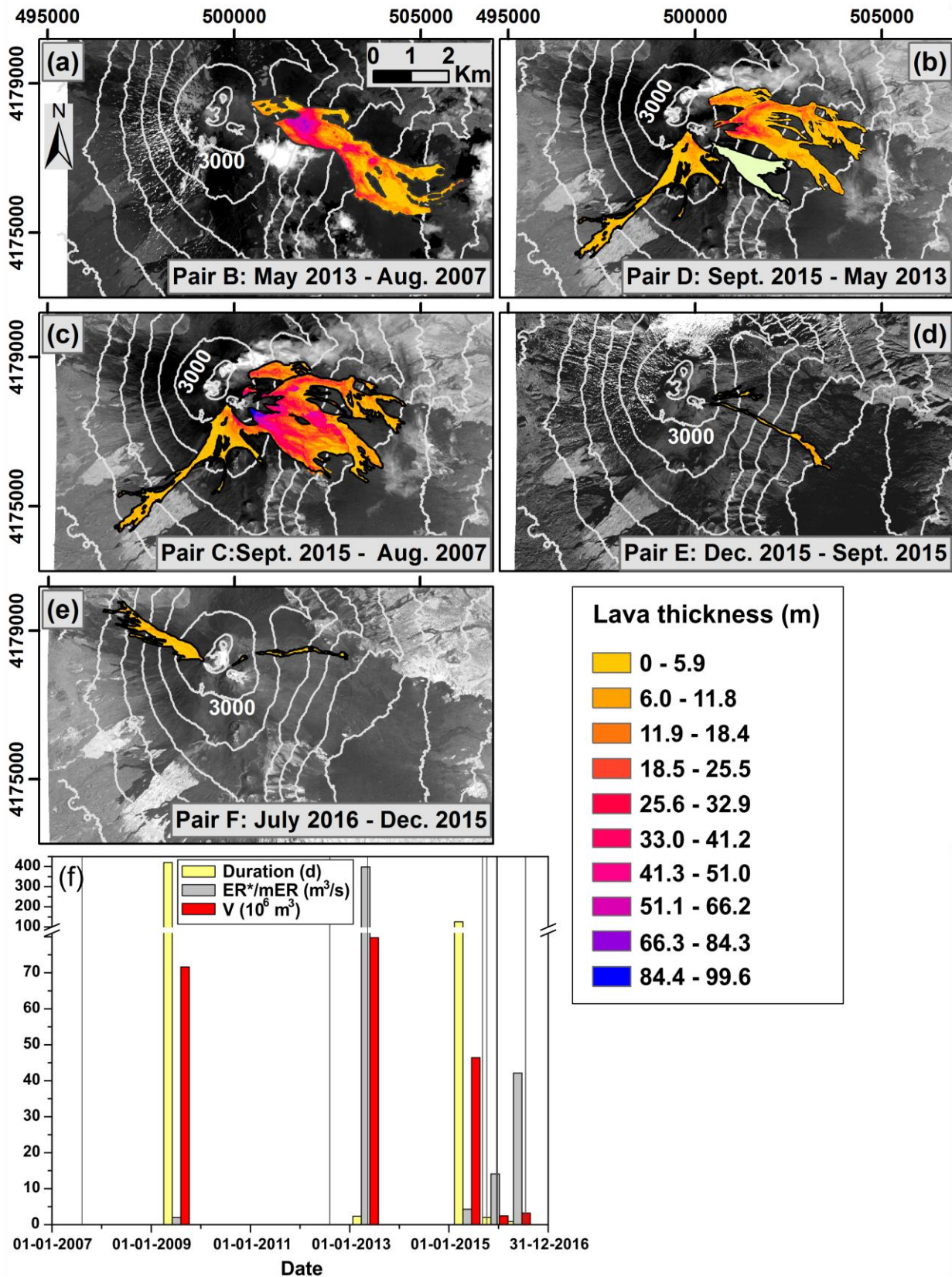
509
 510 **Fig. 2** Duration of the different eruptive events from 2011 to 2013 (a) and from 2014 to 2016 (b). (c) and (d) are enlargements of the
 511 dashed rectangles in (a) and (b). Grey vertical lines indicate the timing of DEM acquisitions.



512
 513 **Fig. 3** Root mean square of the discrepancies between the coordinates, measured on the Pleiades and the 2005 DEMs, for GCPs and
 514 CPs (full triangles and empty circles, respectively).

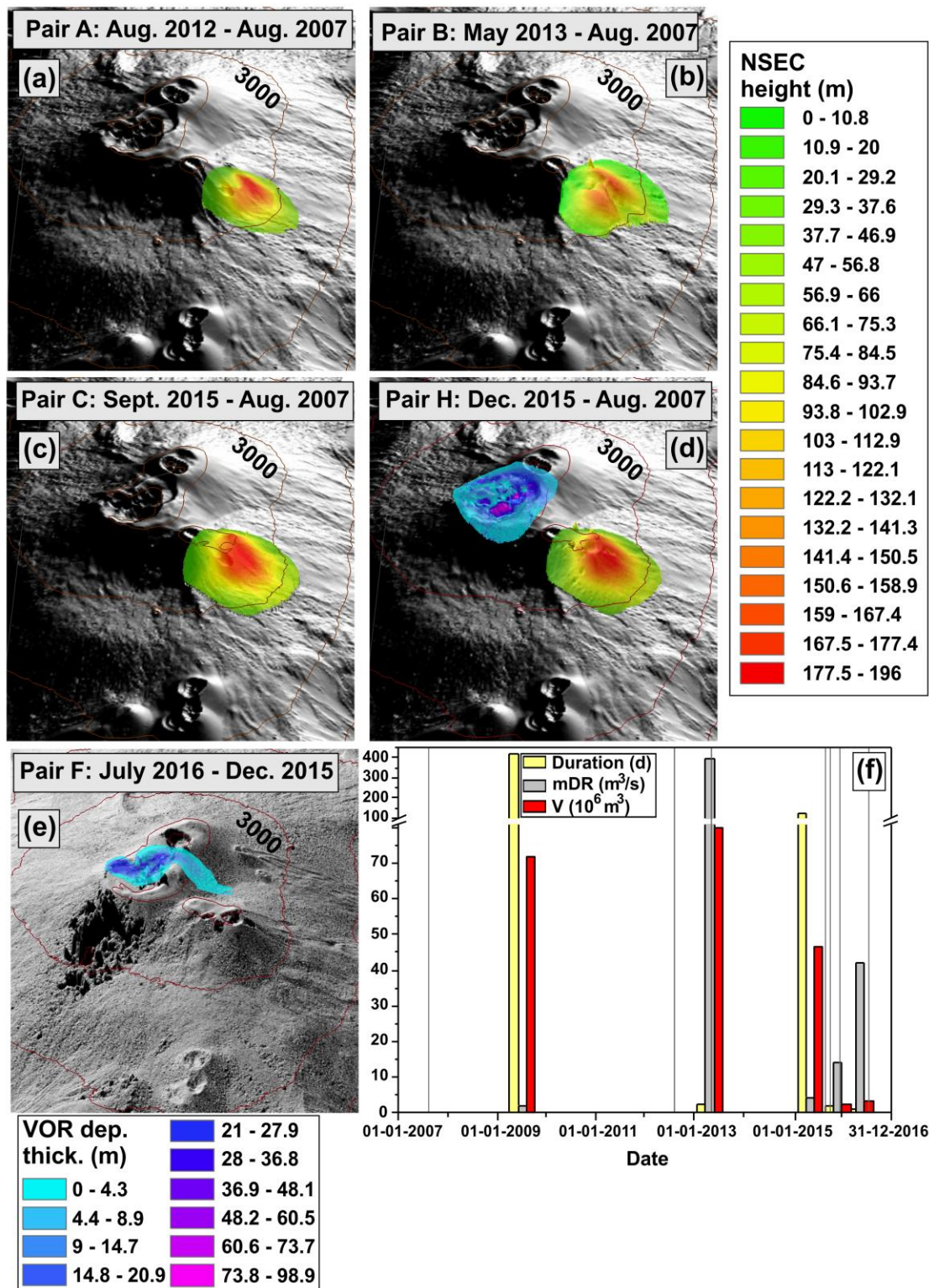


515
 516 Fig. 4 (a-c) Flow fields and check areas shown on orthophotos from 5 September 2015, 18 December 2015 and 18 July 2016. (d)
 517 NSEC cone base and check areas shown on the 2007 shaded relief. E and N coordinates in (a-c) are the same as in (d); scale bars and N
 518 arrow of all maps are the same as in (c). Contour lines of geoid height are drawn every 250 m. (e-h) Distributions of the height residuals
 519 evaluated over the check areas for pairs D, E, and F, as well as for each pair of Pleiades-2007 DEMs, after ellipsoid-geoid correction.

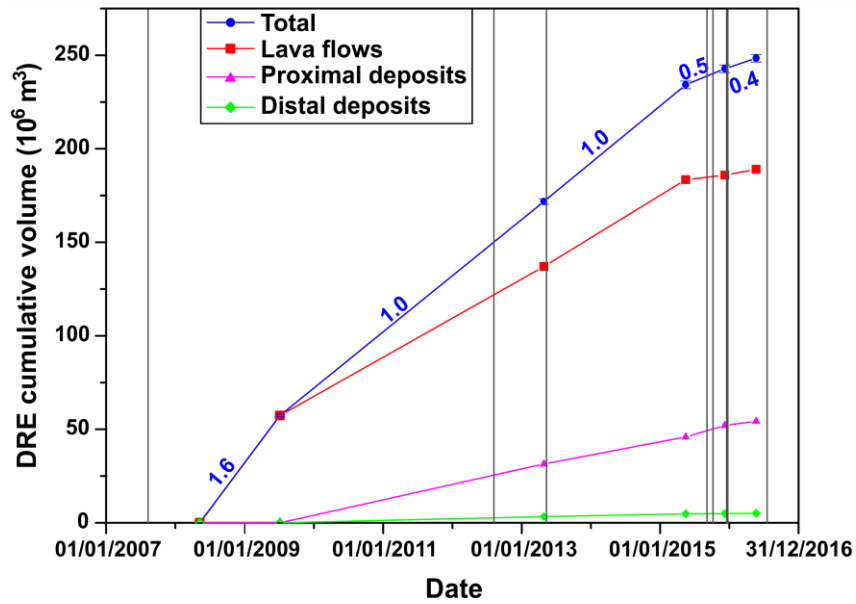


520
521
522
523
524

Fig. 5 (a-e) Thicknesses of the lava flow fields, shown over post-event orthophotos with contour lines of geoid height every 250 m, measured from pairs B, D, C, E and F; coordinate ranges, scale bar and north arrow in (a), as well as thickness scale are the same for all maps. (f) Total volume (V), duration and eruption/multi-event eruption rates (ER*/mER), drawn at the last event in each time interval. Grey vertical lines indicate the timing of DEM acquisitions.



525
 526 **Fig. 6 (a-d)** NSEC cone height measured, with respect to the 2007 DEM (background image), on the August 2012, May 2013,
 527 September and December 2015 DEMs. **(d-e)** Thickness of VOR deposits in December 2015 and between December 2015 and July 2016.
 528 Legends are the same for all maps. Background image in (e) is 2016 shaded relief. Contour lines of geoid height are drawn every 250 m. **(f)**
 529 Duration, volume (V) and multi-event deposition rate (mDR), drawn at the last event in each time interval, for all paroxysms between each
 530 DEM pair. Grey vertical lines indicate the timing of DEM acquisitions.



531
532
533

Fig. 7 Cumulative DRE volumes (drawn at the last event in each time interval) of the different volcanic products. Grey vertical lines indicate the timing of DEM acquisitions. Blue numbers are magma output rate (m³/s) between two volume measurements.